

Hydrogen Physisorption on Metal–Organic Framework Linkers and Metalated Linkers: A Computational Study of the Factors That Control Binding Strength

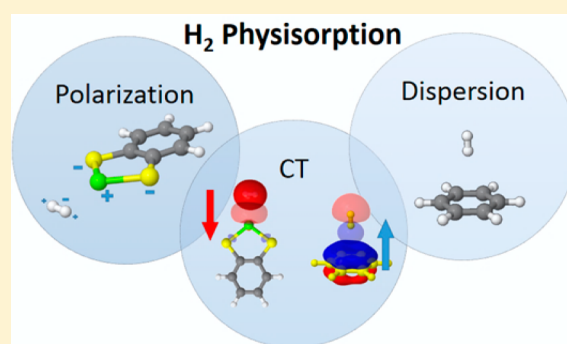
Ehud Tsivion,^{†,§} Jeffrey R. Long,^{†,§} and Martin Head-Gordon^{*,‡,§}

[†]Materials Sciences Division and [‡]Chemical Sciences Division, Lawrence Berkeley National Laboratory, Berkeley, California 94720, United States

[§]Department of Chemistry, University of California, Berkeley, California 94720, United States

S Supporting Information

ABSTRACT: In order for hydrogen gas to be used as a fuel, it must be stored in sufficient quantity on board the vehicle. Efforts are being made to increase the hydrogen storage capabilities of metal–organic frameworks (MOFs) by introducing unsaturated metal sites into their linking element(s), as hydrogen adsorption centers. In order to devise successful hydrogen storage strategies there is a need for a fundamental understanding of the weak and elusive hydrogen physisorption interaction. Here we report our findings from the investigation of the weak intermolecular interactions of adsorbed hydrogen molecules on MOF-linkers by using cluster models. Since physical interactions such as dispersion and polarization have a major contribution to attraction energy, our approach is to analyze the adsorption interaction using energy decomposition analysis (EDA) that distinguishes the contribution of the physical interactions from the charge-transfer (CT) “chemical” interaction. Surprisingly, it is found that CT from the adsorbent to the $\sigma^*(\text{H}_2)$ orbital is present in all studied complexes and can contribute up to approximately -2 kJ/mol to the interaction. When metal ions are present, donation from the $\sigma(\text{H}_2) \rightarrow$ metal Rydberg-like orbital, along with the adsorbent $\rightarrow \sigma^*(\text{H}_2)$ contribution, can contribute from -2 to -10 kJ/mol, depending on the coordination mode. To reach a sufficient adsorption enthalpy for practical usage, the hydrogen molecule must be substantially polarized. Ultimately, the ability of the metalated linker to polarize the hydrogen molecule is highly dependent on the geometry of the metal ion coordination site where a strong electrostatic dipole or quadrupole moment is required.



INTRODUCTION

Hydrogen (H_2) gas is a promising candidate for future use as an energy carrier for mobile applications such as vehicles and aircrafts. Hydrogen has almost three times higher gravimetric energy content than gasoline, and its combustion or utilization in a fuel cell is a “zero emission” process that results in the formation of water without emitting any compounds that pollute the environment or disrupt the climate. Since H_2 is an extremely volatile gas under standard conditions, the energy available per unit volume (volumetric energy density) is too low for practical application, requiring its storage at high pressures or as a liquid at cryogenic temperatures on board a vehicle. An efficient method for the storage of H_2 is therefore a necessary technology for its effective use as a fuel. The 2017 DoE target values for an onboard hydrogen storage system for light-duty fuel cell vehicles are a gravimetric capacity of 5.5 wt % ($\text{kg H}_2/\text{kg}$) and a volumetric capacity of 4.0 vol % ($\text{kg H}_2/\text{L}$) at an operating temperature of -40 to 60 °C. To the best of our knowledge, these targets have yet to be met by any known material upon incorporation into a storage system.

Metal–organic frameworks (MOFs) are a family of compounds consisting of metal ions or clusters coordinated to organic ligands (linkers), which form extended network structures. These materials have attracted attention for their potential use as gas-storage media.¹ MOF structures often have sizable pores that can be filled with guest molecules, many of which are adsorbed to the internal surfaces. Moreover, the MOF composition and structure can be modified and tuned for many purposes,² such as catalysis³ and chemical separations.^{1,4}

A reversible mechanism for adsorption and release of H_2 from its storage material is needed for any practical storage application. In this respect, the weak physisorption of H_2 in MOFs is advantageous, since H_2 can reversibly adsorb to pore surfaces within the MOF and be easily released when needed. However, the weak adsorption enthalpy (H_{ads}) of H_2 to most known MOFs poses a challenge. At ambient temperatures, an adsorption enthalpy of -15 to -20 kJ mol⁻¹ is needed for optimum hydrogen storage–delivery cycles depending upon

Received: October 7, 2014

Published: November 21, 2014

the minimum and maximum allowed pressure of the system, while most H_{ads} values for MOFs are in the range of -5 to -12 kJ/mol.⁵

A promising path for increasing the H_2 adsorption capabilities of MOFs is the functionalization of their organic linking components⁶ to incorporate stronger adsorption sites by applying postsynthetic modifications.⁷ In this approach, functionalized groups are introduced into the MOF after it has already been prepared, such that the sensitive preparation process of the MOF is not disrupted by their presence. In particular, efforts are being made to produce MOFs containing sites capable of being postsynthetically metalated with low-coordinate or partially exposed metal cations^{8,9} that are known to be an excellent H_2 adsorption centers.^{10–12}

The primary goal of this paper is to present a fundamental investigation into the physisorption mechanism of hydrogen on MOF linkers and metalated MOF linkers in order to understand the chemical principles which influence the overall adsorption. Once these are understood, we are able to provide some guidelines for preparation of successful hydrogen adsorbing linkers based on the implications of our results.

Chemistry of Hydrogen. The hydrogen molecule has low chemical activity. Because of its low-lying σ_g orbital and a high-lying σ_u^* orbital, it does not readily donate or receive electrons. Exceptions are the well-known dihydrogen “Kubas” complexes,¹³ where a hydrogen–metal complex is formed by a synergetic mechanism (Figure 1) where a hydrogen molecule

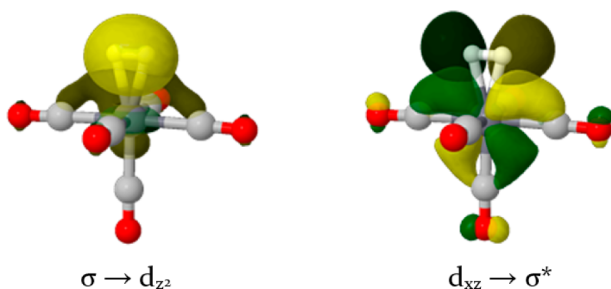


Figure 1. Chemical bonding in a dihydrogen “Kubas” complex $\text{Cr}(\text{CO})_5(\text{H}_2)$. Donor and acceptor orbitals are opaque and partly transparent, respectively.

donates density from its filled σ_g orbital into an empty d orbital of the metal, $\sigma(\text{H}_2) \rightarrow d(\text{M})$, and the metal back-donates electronic density to the σ^* orbital $\sigma^*(\text{H}_2) \leftarrow d(\text{M})$.^{14,15} However, the binding enthalpy for these complexes can be as high as ~ 80 kJ/mol, which is too strong for mobile hydrogen storage applications; therefore, other forms of interactions should be exploited. Also, the interaction of hydrogen with many other open-shell metal species is too strong for hydrogen storage applications.^{16,17}

Unlike chemically bound dihydrogen complexes, hydrogen physisorption is not considered to be a “chemical” process in the sense of formation/breakage of chemical bonds which involves significant charge transfer interactions and changes in electronic structure. Rather, physisorption is a much weaker interaction that primarily involves contributions from electrostatic (both permanent and induced electric moments) and dispersion interactions, considered to be physical in nature.

What are the factors involved in hydrogen adsorption? (1) Hydrogen has a permanent quadrupole moment, which is a product of the accumulation of charge-density in between the two H atoms through the formation of a chemical bond. This

electric moment can interact with electric fields within the MOF environment. (2) Hydrogen is a “hard” molecule with a HOMO–LUMO gap of about 11.19 eV, and therefore is not likely to be significantly polarized by electric fields in the MOF unless they are strong. Thus, the incorporation of exposed metal cations with high charge-density within the MOF is expected to have significant polarization interaction with the H_2 .^{12,18} (3) Although also challenged by the large HOMO–LUMO gap, some charge-transfer (CT) interaction could occur between the hydrogen and its substrate. Moreover, any CT interaction that occurs between hydrogen and its absorbent could potentially reduce the gap and increase the strength of polarization interactions and vice versa.

This article is organized as follows: The next section discusses the computational approach taken, followed by a section that discusses the fundamental aspects of hydrogen adsorption by analyzing adsorption interactions in small model clusters. Subsequently, two sections are dedicated to physisorption on larger, more realistic systems, which show H_2 adsorption energies ranging between weak and relatively strong. The article concludes with a discussion of the fundamental mechanisms of H_2 physisorption and their implications for the design of H_2 adsorbing materials.

■ COMPUTATIONAL SECTION

Model. H_2 adsorption on a MOF linker is modeled using a molecular species consisting of H_2 and the host ligand. While MOFs are infinite extended structures, they are composed of well-defined ligand subunits that, to a reasonable approximation, maintain their individual precursor (pre-MOF) structures. Even though cluster models are very different from an extended MOF, one must keep in mind that the H_2 molecule bond length is only 74 pm long, shorter than a typical C–H bond. Hence, H_2 adsorption is a local interaction which is mainly sensitive to the immediate environment of the adsorption sites. Cluster models should therefore be able to provide a reliable description of the adsorption interactions and yield valuable insights. This hypothesis is supported by numerous successful previous studies.^{12,19–25}

While the present work is focused on MOF linkers, one should also be interested in the contribution from MOFs featuring coordinatively unsaturated metal ions to the overall H_2 adsorption: These metal centers themselves can have a considerable influence on the overall H_2 adsorption and are generally expected to have stronger interactions with H_2 than a bare ligand. For instance in MOF-5,²⁶ well-known for its excellent cryogenic H_2 adsorption capabilities, it was found that the strongest H_2 adsorption sites are located at pockets, or corners, adjacent to the cluster nodes (“ α -sites”), with an adsorption enthalpy of approximately -7 kJ/mol.²¹ However, since the interaction of any fully coordinated metal with H_2 is arguably insufficient for practical storage purposes, it is therefore more constructive to focus our attention on the linkers that could potentially be modified to have sufficient interaction.

The experimentally relevant thermodynamic quantity for the adsorption of H_2 is the differential enthalpy of adsorption (ΔH_{ads}). For the case of H_2 adsorption, the major contribution to H_{ads} , other than the electronic energy, originates from the restrictions of the H_2 movements once adsorbed. ΔH_{ads} is reported for the experimentally relevant larger models.

Inelastic neutron scattering experiments indicate that H_2 retains one out of its two rotational degrees of freedom upon adsorption to a metallic center in MOFs.^{27–30} We therefore assume that same phenomena occurred also for the weakly interacting systems, studied here. This approach had been successfully employed for the prediction of H_2 adsorption isotherms in MOF-5.²¹ The same cannot be assumed, without experimental evidence, for strongly adsorbed H_2 , where the strong electrostatic interactions require specific orientations of the H_2 molecule. However, assuming that the H_2 molecule retains at

least some of its rotational or translational degrees of freedom even for the strongly interacting systems, we estimate that results provided here underestimate ΔH_{ads} by approximately 1–3 kJ/mol for these cases.

Energy Decomposition Analysis. The physisorption interaction of H_2 is essentially nonchemical, and therefore standard wave function analysis concepts, such as partial charges and bond orders, would not provide a sufficiently detailed picture of the underlying chemistry. Our computational approach is to employ “energy decomposition analysis”^{31,32} (EDA) as implemented in the Q-Chem quantum chemistry package,³³ which decomposes the intermolecular interactions of two or more interacting molecules, into three basic contributions: (1) Frozen (FRZ), (2) Polarization (POL), and (3) Charge-Transfer (CT).

$$E_{\text{interaction}} = E_{\text{FRZ}} + E_{\text{POL}} + E_{\text{CT}}$$

The FRZ term corresponds to the energy change due to interactions that are not related to a change in electronic density of the interacting molecule, i.e., electrostatic interactions due to permanent multipoles, dispersion and steric repulsion. The POL term corresponds to the energy change due to the polarization of the density of each molecule, while remaining localized on the molecule. The CT term corresponds to energy change due to the flow of charge between the polarized molecules.

Our implementation of the EDA analysis relies on an SCF procedure known as “SCF-MI”^{34,35} for obtaining an “absolutely localized molecular orbital” (ALMO) wave function Ψ_{ALMO} . The ALMOs are variationally optimized to be localized on each of the molecules, such that CT from one molecule to another is excluded, by fragment-blocking the MO coefficient matrix. Each of the energy components is evaluated in the following way: The FRZ term is evaluated as the energy required to bring infinitely separated molecules into the complex geometry, using the frozen MOs of the fragments: $E_{\text{FRZ}} = E(\Psi_0) - \sum_x E(\Psi_x)$. The POL term is evaluated as the difference between the energy of the optimized ALMO wave function and the nonrelaxed frozen wave function of the complex: $E_{\text{POL}} = E(\Psi_{\text{ALMO}}) - E(\Psi_0)$. The CT term is evaluated as the energy difference between the energy of the fully converged SCF wave function of the complex and the CT-excluded ALMO energy: $E_{\text{CT}} = E(\Psi_{\text{SCF}}) - E(\Psi_{\text{ALMO}})$.

The positive energy related to the geometric distortion of the molecule in its complex geometry with respect to its isolated geometry is called the “geometric distortion” (GD) energy. In the context of hydrogen adsorption, this energy is very small or even completely negligible—often less than 0.5 kJ/mol; therefore, it is generally omitted for the sake of clarity.

This work also employs the complementary occupied–virtual orbital pairs (COVPs)³⁶ for visualization of the intermolecular CT interactions. COVPs are a chemical representation of intermolecular CT in simple terms of donor–acceptor orbital pairs that provide a compact representation of the most significant donor–acceptor orbital interactions.

Computational Details. The B97-D functional³⁷ with empirical dispersion correction³⁸ (D3) along with def2-tzvpd basis set^{39,40} is used for structure optimization, frequencies and vibrational analysis. The ω B97X-V functional⁴¹ along with def2-qzvp basis set is used for calculations of interaction energies and EDA analysis with no counterpoise correction for basis set superposition error. The ω B97X-V/def2-qzvp combination is expected to yield a statistical error of 0.5 kJ/mol, as benchmarked against the A24 data set for noncovalent interactions.⁴² We estimate that an additional error of approximately 1 kJ/mol, related to the evaluation of thermal properties, is expected for enthalpy. Structures are optimized and verified to be a minimum on the potential energy surface with zero negative eigenvalue of the Hessian.

Comparing the EDA results obtained using the ω B97X-V functional with the B3LYP-D3 functional^{35,39} the absolute adsorption energies agree within approximately 10%: ~ 0.4 kJ/mol for the nonmetallic linkers and ~ 2 kJ/mol for the strongly absorbing linker. For the weakly absorbing metallic linkers, larger differences of ~ 3 kJ/mol are found, mostly due to large differences in the evaluation of the frozen

term and thus to the differences in the different approaches for the evaluation of the dispersion (D3³⁸ vs VV10 nonlocal functional⁴³). For aluminum compounds, B97-d3 predicted considerably weaker adsorption energies, with respect to the other functionals, hence the ω B97X-V functional was used also for their structure optimization.

Additional details regarding the basis-sets used for the PCM18-NiCl₂ model, DFT functional comparison for the aluminum compounds and optimized structures are given in the Supporting Information.

RESULTS

Contributions to H_2 Physisorption. Nonmetallic Linker– H_2 Interactions. MOFs are constructed from metal ions or clusters linked by organic ligands, known as “linkers”. Although the H_2 –linker adsorption interaction is known to be small, it demonstrates the most basic interactions of physisorbed H_2 and is therefore important for having a complete picture of the interactions of H_2 molecules within a MOF. The optimized structures obtained for the clusters of H_2 with organic molecules, representing the most basic and common building blocks for MOF-linkers (a) benzene, (b) phenol, (c) terephthalic acid (BDC), and (d) tetrazole, are shown in Figure 2 and the EDA for the interaction of these complexes is shown in Table 1.

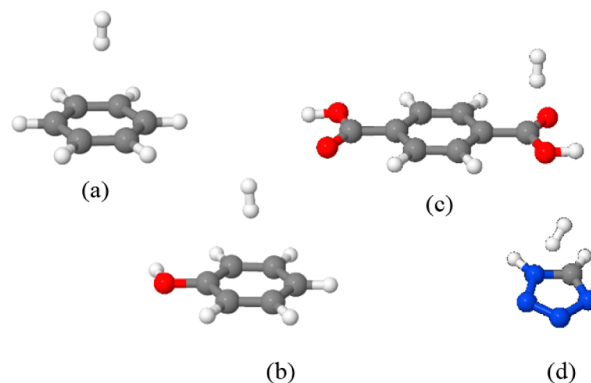


Figure 2. H_2 physisorbed on MOF linker-like molecules: (a) benzene, (b) phenol, (c) BDC, (d) tetrazole.

Table 1. Energy Decomposition Analysis of H_2 –Linker Interactions [kJ/mol]

	benzene	phenol	BDC	tetrazole
Frozen	−2.7	−2.7	−1.7	−1.8
Pol.	−0.5	−0.5	−0.3	−0.1
CT	−1.2	−1.3	−1.6	−0.5
Total (ΔE)	−4.4	−4.5	−3.7	−2.4

The frozen and CT terms are the most dominant interactions in the complexes. The frozen interactions could be traced to London dispersion interactions which are long-range interactions that are highly sensitive to the interatomic distance ($\sim 1/R^6$). In order to maximize the London interactions, the H_2 molecule is positioned in the vicinity of as many atoms as possible: the center of the aromatic ring (benzene and phenol) or the middle of a chain (butane).

Perhaps surprisingly, CT interactions are important for the adsorption interaction and are significant for all of the complexes. Unlike the frozen interactions, CT interactions can be directly associated with the electronic structure of H_2 and the linker and can be assigned to specific donor–acceptor

orbitals. The results of the qualitative analysis for CT in H₂–ligand complexes are shown in Figure 3.

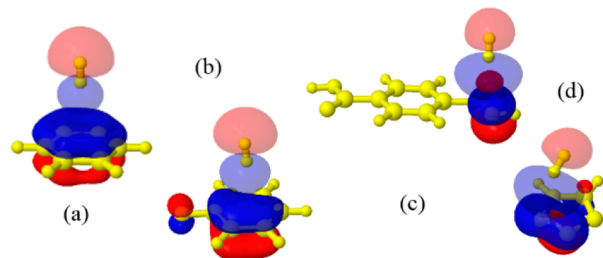


Figure 3. Adsorbent $\rightarrow \sigma^*(\text{H}_2)$ charge transfer in H₂ physisorption. Donor and acceptor orbitals are opaque and partly transparent, respectively. Panels (a–d) correspond to (a) benzene, (b) phenol, (c) BDC, (d) tetrazole, as in Figure 2.

It can be observed that the donor orbitals on the ligands have p or π (conjugated p) character, that expands out of the aromatic ring plane, and are therefore able to have some overlap with the $\sigma^*(\text{H}_2)$ orbital, which is the dominant acceptor orbital in these complexes. There is also some donation from H₂ to the linker, which contributes about 30% of the CT. However, this weaker CT component (not shown) involves delocalized acceptor orbitals on the ligand, which precludes meaningful chemical analysis. The CT interaction has significant influence on the structure of the complex and orientation of the H₂ molecule: The H₂ molecule appears to be spatially positioned to maximize the CT between the H₂ and its adsorbent, oriented heads-on toward the source of electronic density, thereby increasing orbital overlap between the source and $\sigma^*(\text{H}_2)$ accepting orbital.

The adsorption interaction is similar for the heterocyclic compounds. However, in the BDC complex, the H₂ molecule cannot assume the “head-on” position at the center of the ring, due to the presence of negative repulsive charges at both ends of the adsorbate molecule. Hence the frozen interaction component is weaker by 1 kJ/mol with respect to the others.

Polarization interaction is nearly negligible in all complexes due to the low polarizability of H₂ and the absence of highly charged centers on the linkers. It is also an indication of the weakness of the interactions, which results in only minor changes to the electronic structure of the interacting species.

Interaction with the Adsorption Site of a Metal Decorated Linker. To study the adsorption of H₂ on metal-functionalized linkers, we select a series of small molecules that model the adsorption sites of larger, more realistic, systems. The selection of metals is mostly driven by practical considerations: A suitable ion should have an adsorption energy in the desired range (–15 to –20 kJ/mol) and be lightweight, cheap and environmentally benign. Since first-row transition metals are expected to have strong interaction with H₂, we therefore select the Ca, Mg and Al cations that are expected to have relatively weak interactions with H₂ and are also earth-abundant and nontoxic. The optimized structures are shown in Figure 4 and the EDA of the interactions in these complexes are listed in Table 2.

The frozen interactions have a significant contribution for all complexes, which is controlled by the interaction of the electrostatic moments on the H₂ and the relatively ionic adsorbents, and their Pauli repulsion (particularly prominent in AlF₃). The contribution from dispersion interactions is

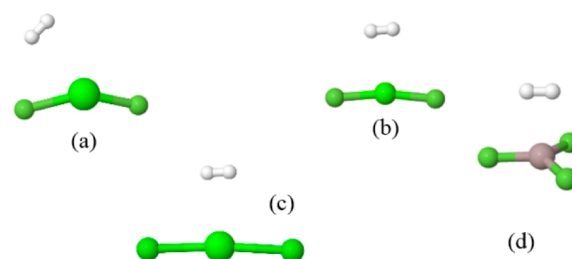


Figure 4. H₂ physisorbed on molecules representing MOF-linker metalated site: (a) CaF₂, (b) CaCl₂, (c) MgCl₂, (d) AlF₃.

Table 2. Energy Decomposition Analysis of Metalated Linker–H₂ Interactions [kJ/mol]

	CaF ₂	CaCl ₂	MgF ₂	AlF ₃
Frozen	–4.3	–5.3	–3.6	17.3
Pol.	–4.5	–5.2	–6.0	–26.4
CT	–3.8	–4.3	–4.9	–15.3
Total (ΔE)	–12.6	–14.8	–14.5	–24.4

expected to be relatively small due to the small number of atoms.

The energy lowering due to polarization is caused by the response of the electronic density of the H₂ molecule, induced by the strong electrostatic moments of the substrate, to form new (or more favorable) electrostatic moments that have an energy lowering interaction with the permanent moments of the substrate. H₂ is expected to cause very little substrate polarization.

The polarization of H₂ can have two forms: (1) Where the H₂ is adsorbed in between a positive and a negative ion (as in CaF₂), one hydrogen atom gains charge density while the other is depleted, inducing a dipole moment. (2) Where H₂ is adsorbed symmetrically, above the positive ion in equal distance from the negative ions, density builds up in between the hydrogen atoms and is symmetrically depleted from the sides, thereby modifying the quadrupole moment. This symmetrical polarization cannot be inferred from conventional atomic density partition approaches (e.g., a Mulliken population analysis), since the density remains approximately equally distributed between the atoms.

Significant factors that influence the polarization interactions are as follows: (1) Metal ions with a small radius allow the hydrogen molecule to move closer to the ion where the electrostatic field is stronger and results in stronger polarization. (2) Since Al has a formal 3+ oxidation state, it generates a stronger electric field that results in stronger polarization.

CT interactions make a contribution of about one-third of the overall complexation energy for the Ca and Mg complexes. The dominant CT interaction is the donation of density from $\sigma(\text{H}_2) \rightarrow$ Rydberg-like orbitals on the metal (Figure 5a). Because of the poor overlap between the diffuse vacant orbitals, CT is relatively small: For example, in CaF₂–H₂ the energy related to CT in the $\sigma(\text{H}_2) \rightarrow 4s(\text{Ca})$ interaction is –1.3 kJ/mol, obtained by the COVP analysis. This is not the case for Al³⁺ where its vacant 3p_z valence orbital is largely responsible for the significantly increased interaction of AlF₃ and H₂. Since the 3p_z(Al³⁺) orbital has good overlap with the $\sigma(\text{H}_2)$ orbital, it readily accepts electron density, resulting in a significantly larger interaction energy: the energy related to CT in the $\sigma(\text{H}_2) \rightarrow 3p_z(\text{Al}^{3+})$ interaction is –5.4 kJ/mol. There is always a smaller back-donation from the formally reduced atoms of the

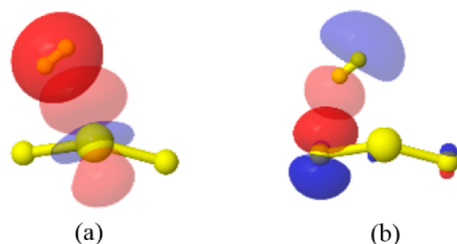


Figure 5. Charge transfer interactions in physisorption of H_2 on metalated sites, as demonstrated by CaF_2 . (a) Forward donation $\sigma(H_2) \rightarrow d(\text{Metal})$ and (b) backward donation lone-pair(Ligand) $\rightarrow \sigma^*(H_2)$. Donor and acceptor orbitals are opaque and partly transparent, respectively.

linker to the antibonding $\sigma^*(H_2)$ orbital (Figure 5b), similar to what was encountered in the previous section on bare-linker interactions.

The AlF_3-H_2 complex displays a different interaction picture than the other complexes, which is closer to the characteristics of a chemical bond: the strong polarization and CT interactions indicate significant changes in the electronic structure, while the repulsive frozen interaction indicates a close proximity of the interacting species.

Vibrational Spectroscopy. Vibrational spectroscopy can provide an important connection between experiment and the calculated adsorption characteristics of the complexes. Since the H_2 molecule lacks a dipole moment, it is not active in the IR spectra. However, adsorbed H_2 molecules can be activated in the IR as seen by the predicted values in Table 3.

For the H_2 bare-ligand complexes that are bound mostly by London and weak CT forces, there is only a minor shift in the stretch frequency with respect to isolated H_2 , which is caused by the small degree of linker $\rightarrow \sigma^*(H_2)$ CT. For the H_2 -metal complexes, there is a stronger red shift in the H–H stretch of approximately 100 cm^{-1} , due to the transfer of some electron density from the bonding $\sigma(H_2)$ orbital to the metal.

What is the mechanism of activation in the IR spectra? The selection rule requires a nonzero dipole derivative. For the strongly polarized complexes such as CaF_2 , a dipole moment is formed by asymmetric polarization of the adsorbed H_2 , where each H atom gains a different charge. Therefore, for symmetrically adsorbed H_2 molecules, such as with $CaCl_2$ where only a quadrupole moment is formed, the activation is weaker. For the bare-ligand complexes, where no significant polarization mechanism exists, there is a different IR activation mechanism: When the H_2 molecule vibrates one of the H atom moves closer to the electron cloud on the substrate, gaining some negative charge and increasing the dipole moment of the H_2 . Therefore, the H_2 is activated dynamically by a vibrational induction mechanism.

Weakly Absorbing Metalated Linkers. Now that the physisorption of H_2 was studied for small clusters representing key parts of a MOFs linker, H_2 physisorption on larger models, representing more realistic MOF-linker systems of interest, is investigated. The three metalated linker-like complexes evaluated (shown in Figure 6) are isostructural to MOF linkers

Table 3. IR Spectroscopic Properties of Adsorbed H_2

	isolated H_2	$H_2@CaF_2$	$H_2@CaCl_2$	$H_2@phenol$	$H_2@benzene$
$\nu(H-H)$ [cm^{-1}] (red shift)	4378.2 (0.0)	4295.6 (82.5)	4286.2 (92.0)	4364.7 (13.4)	4366.5 (11.6)
Intensity [km/mol]	0	12.1	3.8	18.4	17.8

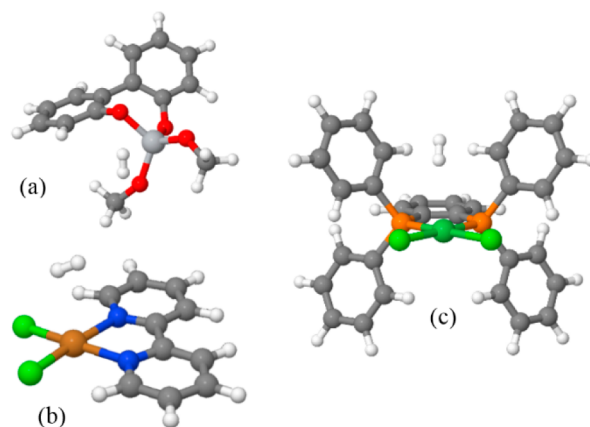


Figure 6. Weakly interacting complexes of H_2 with metalated linkers: (a) Biphenyl- (TiO_4) -dimethyl, (b) bpy- $CuCl_2$, (c) PCM $_{18}$ - $NiCl_2$.

that have been reported in the literature to be metalated. They are predicted here to be weak H_2 adsorbents, and thus inadequate for practical storage applications.

Biphenyl- (TiO_4) -dimethylene. The first system considered here is based on a linker derived from 1,1'-bi-2-naphthol (BINOL), which is the linking element of CMOF-3b, reported to be metalated using $Ti(O^iPr)_4$.⁴⁴ We use biphenyl- (TiO_4) -dimethyl as a model for the experimentally obtained linker (Figure 6a). Our model neglects the effect of the distant aromatic rings and isopropyl groups while retaining the structure of the metal site on the linker, at which the strongest H_2 binding is expected to occur. The Ti^{4+} ion is tetrahedrally coordinated by four oxygen atoms, meaning that the metal is only marginally accessible by H_2 for CT interactions, which are therefore expected to be weak. However, the H_2 is oriented “side-on” toward the metal ion, implying some CT interaction. Another implication of the tetrahedral coordination of the Ti atom is that no strong low-order electrostatic moments are available for polarization interactions with the H_2 .

Indeed, the EDA analysis (Table 4) verifies this qualitative analysis: CT is small but non-negligible, contributing -1.5 kJ/

Table 4. Energy Decomposition Analysis of H_2 Binding to Metalated Linkers [kJ/mol]

	biPh- TiO_4	bpy- $CuCl_2$	PCM18- $NiCl_2$
Frozen	-2.4	-0.8	-1.7
Pol.	-0.8	-1.9	-2.2
CT	-1.5	-2.8	-4.8
Total (ΔE)	-4.7	-5.5	-8.7
ΔH_{ads}	-3.6	-4.4	-7.9

mol to the interaction. The CT could be traced to weak $\sigma(H_2) \rightarrow$ metal donation (hence the “side-on” position) and back-donation, linker $\rightarrow \sigma^*(H_2)$. The frozen interaction is the largest of the interactions and contributes -2.4 kJ/mol . It originates in both dispersion and permanent electrostatic interactions of the H_2 with the adsorption site atoms. The polarization interaction is very weak due to the absence of strong electrostatic

moments. Overall, the metalated BINOL linker is calculated to have a very weak H_2 adsorption enthalpy of only -3.6 kJ/mol and is the weakest of the studied linkers.

bpy-CuCl₂ (10). 2,2'-Bipyridine (bpy) is one of the most widely used ligands in coordination chemistry due to its strong affinity for metals. It is also commonly used as a MOF linking element and there are several reports in the literature of MOFs containing metalated bpy units.^{8,45,46} Here we use a model composed of a bpy ligand metalated by $CuCl_2$, forming a planar structure (Figure 6b) with the Cu^{2+} ion exposed along the z axis. The existence of a partially exposed metal site is expected to allow for stronger CT interactions between the Cu and the H_2 molecule, since better overlap is expected to occur between the diffuse empty orbitals of the metal and the occupied $\sigma(H_2)$ orbital.

The EDA analysis (Table 4) indicates that CT in this complex contributes -2.8 kJ/mol to the overall electronic interaction energy, larger than -1.5 kJ/mol for the tetrahedral complex discussed above. The important CT contributions are the $\sigma(H_2) \rightarrow$ metal contribution (Figure 7a) and the back-

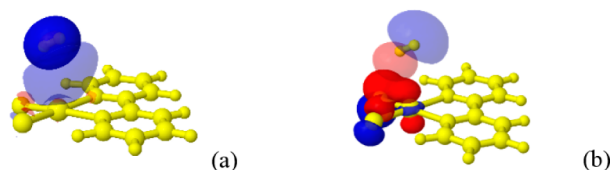


Figure 7. Charge transfer interactions in $H_2@bpy-CuCl_2$, which is a weakly interacting complex. Donor and acceptor orbitals are opaque and partly transparent, respectively.

donation from the orbitals of $p_z(Cl)$ and $d_{z^2}(Cu)$ to $\sigma^*(H_2)$ (Figure 7b). Forward and backward donations have roughly equal importance. These are essentially the same CT interactions that have appeared in the small model of $H_2@CaF_2$. The role of the $\sigma(H_2) \rightarrow$ metal CT interaction can be inferred by observing the geometry of the complex in Figure 6b: The H_2 molecule is oriented “side-on” toward the transition metal, maximizing donation to the metal. At the same time it is also slightly tilted with respect to the plane to maximize linker $\rightarrow \sigma^*(H_2)$ CT.

The contribution of polarization is -1.9 kJ/mol, which is more than two times larger compared to -0.8 kJ/mol for the tetrahedral complex. The increase in polarization is likely enabled by H_2 experiencing nonzero (though still small) local electrostatic moments around the Cu^{2+} ion.

The overall ΔH_{ads} of H_2 is only -4.4 kJ/mol, demonstrating that the existence of a partially exposed site by itself is not a sufficient condition for a strong interaction with H_2 .

PCM-18-NiCl₂. A different kind of MOF shown to contain a square planar exposed metal site is PCM-18, which is prepared from premetalated 1,2-substituted bis(phosphines) linkers.⁴⁷ Here, we use a model composed of $NiCl_2$ at the metal site and the adjacent aromatic rings, as shown in Figure 6c. The EDA analysis of the H_2 adsorption is quite similar to the case of $bpy-CuCl_2$; however, there is increased CT, which adds about -2.0 kJ/mol to the overall interaction. This CT interaction originates from a back-donation from the aromatic rings that surround the metal site to the H_2 (Figure 8). Accordingly, the H_2 molecule is not oriented “side-on” toward the metal, but rather is disposed toward the aromatic rings, thereby maximizing CT. The overall ΔH_{ads} of H_2 is -7.8 kJ/mol,

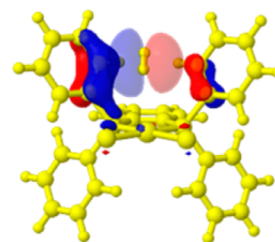


Figure 8. MOF $\rightarrow H_2$ charge transfer in $H_2@PCM_{18}-NiCl_2$: charge is donated from the aromatic rings of the linker to the H_2 . Donor and acceptor orbitals are opaque and partly transparent, respectively.

almost double that calculated for $bpy-CuCl_2$, but still well below the desired target range.

Using transition metals from the second or third row is not expected to have a favorable effect on the adsorption of H_2 . Since polarization is the dominant interaction for strongly physisorbed H_2 , the heavier transition metals have larger radii and are therefore less polarizing. Also, no significant increase in CT is expected, as CT between closed-shell species is always relatively small. However, since the geometry of coordination environment can change (for instance the distance between the metal and the counterions), differences in binding energy are expected. To provide a quantitative measure, the Ag analogue $bpy-AgCl_2$ and Pd analogue $PdCl_2-PCM_{18}$, are found to have an H_2 adsorption energy lower by 3.5 and 2.9 kJ/mol with respect to $bpy-CuCl_2$ and $NiCl_2-PCM_{18}$ (B97-D3/def2-tzvpd).

Strongly Absorbing Metalated Linkers. It has been shown above that the existence of a metal center is by itself not a sufficient condition for strong H_2 binding. In this section we discuss several metalated-linker models that are predicted to bind H_2 more strongly via “physical” interactions and analyze the conditions that give rise to this situation. The linkers discussed are based on the catechol ligand, which is a widely used chelating agent throughout coordination chemistry, or its sulfur-based analogue, 1,2-benzenedithiol. These ligands are shown to be capable of forming highly polar metal coordination complexes that have stronger H_2 adsorption properties. H_2 storage in MOFs composed of metalated catechol linkers was previously studied by Sun and co-workers⁴⁸ and Snurr and co-workers.^{49,50} Our results on the adsorption energies H_2 on cat-Mg are in excellent agreement of less than 1 kJ/mol with their calculations.

MOFs containing catechol ligands were recently synthesized and metalated by Fe^{3+} and Cr^{3+} .^{51,52} However, the specific metalations discussed here have yet to be attained and several synthetic challenges are involved in their preparation. Computational models are used here to demonstrate the principles of successful H_2 adsorbing systems. The optimized structures of the complexes are shown in Figure 9. It can be seen that the adsorption site of the H_2 on the model linkers has a structure that is isoelectronic with the MX_2 or AlF_3 studied above; therefore, the EDA of their interaction with H_2 should also be similar.

The results of the EDA analysis are shown in Table 5. The catechol ligands behave differently from the metalated linkers discussed previously. The main difference is the presence of a much stronger polarization interaction with H_2 ; i.e., the catechol-based compounds have a much greater ability to induce electrostatic moments in the H_2 molecule.

What is the origin of the ability to polarize H_2 ? The catechol linkers have a strong dipole moment that originates from the

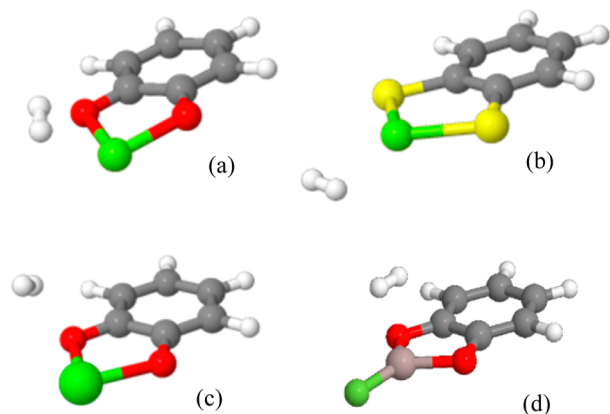


Figure 9. Complexes showing a strong H_2 physisorption interaction: (a) catechol-Mg, (b) 1,2-benzenedithiol-Mg, (c) catechol-Ca, (d) catechol-AlF.

coordination environment of the metal ion: The metal ion is surrounded only by two formal negative charges, placed on both sides of the linker, and thus a strong (local) dipole moment is formed by the combination of negative oxygen/sulfur atoms and the positive metal. We emphasize, that the term “electrostatic moment” is not the global molecular moment, but rather a local moment experienced by the H_2 molecule, which is very small compared to the complexes. Because of its small size, the H_2 molecule is sensitive to localized electrostatic moments, which can and will vary substantially from one place to another on the same linker. These considerations will likely become more important for larger linkers. The local nature of dipole–dipole interactions was recently demonstrated for substituent effects in non-covalent stacking interactions between aromatic rings, where it was shown that the intermolecular dipole–dipole interactions are unperturbed by changes to distant parts of the molecule.^{53,54}

Magnesium is found to be a significantly stronger polarizer of H_2 than calcium, implying an important role for the ionic radius of the metal: all else being equal, smaller is better.

As demonstrated previously on small model molecules, CT also makes an important contribution to the interaction energy, where the $\sigma(H_2) \rightarrow$ metal forward donation is dominant, followed by weaker linker $\rightarrow \sigma^*$ (oxygen to the H_2) back-donation. For 1,2-benzenedithiol-Mg (bdt-Mg), the linker $\rightarrow \sigma^*$ back-donation from the sulfur is smaller than the back-donation in the oxygen-analogues.

CT determines the location of the H_2 molecule: H_2 is oriented “side-on” to the metal to maximize $\sigma \rightarrow$ metal donation (Figure 10a), and if significant linker $\rightarrow \sigma^*$ back-

donation potentially occurs H_2 is positioned closer to the ligand donor (Figure 10b).

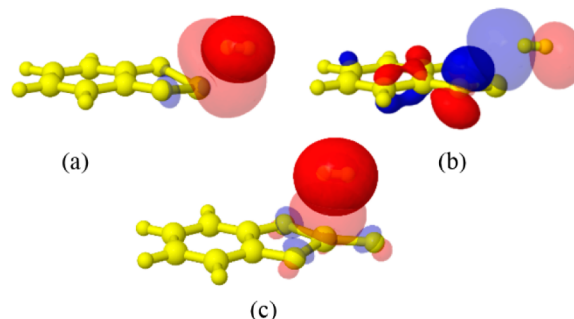


Figure 10. Charge transfer interactions in strongly interacting H_2 adsorbents. Panels (a) and (b) show forward- and back-donation in cat-Mg, while panel (c) shows forward donation in cat-AlF. Donor and acceptor orbitals are opaque and partly transparent, respectively.

The overall H_2 adsorption enthalpy (ΔH_{ads}) of cat-Mg and 1,2-benzenedithiol-Mg is -18.6 and -18.9 kJ/mol, within the DOE target. The calcium based cat-Ca complex has a weaker ΔH_{ads} of -11.1 kJ/mol.

Catechol-AlF. Metalation of the catechol ligand by aluminum deserves special attention for two reasons: (1) It is shown above that AlF_3 is predicted to have an especially strong interaction with H_2 of about -24.4 kJ/mol, greater than the MX_2 compounds. (2) Certain aluminum compounds ($AlCl_3$, $AlBr_3$ and Al_2Me_6) have a significant vapor pressure within the temperature stability range of typical MOFs, and therefore could be used to introduce aluminum into the MOF in the gas phase, as demonstrated by Mondloch and co-workers.⁵⁵ We therefore study an AlF_3 like system in which the two oxygen atoms of the catechol along with a single F^- counterion form a sp^2 hybridized Al^{3+} ion, as shown in Figure 9d.

Catechol-AlF is found to have a strong ΔH_{ads} of approximately -14.1 kJ/mol. The large and positive frozen interaction (Table 5) indicates that the adsorption interaction has some chemisorption character: The frozen energy is repulsive due to the interpenetration of the reactants into each other’s atomic radius. The strong polarization and CT interactions originate from the rearrangement of the electronic structure of the reactants due to the formation of a new dative bond between the occupied $\sigma(H_2)$ and the vacant $p_z(Al^{3+})$ orbital (Figure 10c). The strong quadrupole moment formed by the coordination environment of the Al^{3+} ($O^- - Al^+ - F^-$) is also expected to contribute significantly to the interaction energy, however we are not able to distinguish between the relative contributions of each of the polarization mechanisms.

Table 5. Energy Decomposition Analysis: Catechol Ligands [kJ/mol]^a

	Bdt-Mg	Cat-Mg	Cat-Ca	Cat-AlF
Frozen	-1.8	2.1	-1.3	17.3
Pol.	-11.1	-16.0	-7.7	-22.1
CT	-6.7	-9.1	-6.1	-14.4
Total (ΔE)	-19.6	-23.0	-15.1	-19.3
ΔH_{ads}	-18.9	-18.6	-11.1	-14.1
$\nu(H-H)$ [cm^{-1}] (red shift)	4277.7 (101.5)	4154.0 (224.2)	4210.6 (167.6)	4295.5 (82.7)
Intensity [km/mol]	44.1	30.4	119.7	28.6

^aBdt = 1,2-Benzenedithiol. Cat = Catechol.

DISCUSSION AND CONCLUSIONS

While the (strong) chemical bond is well studied, the chemistry of the very-weak interactions is far less well understood. Recent attempts to prepare hydrogen storage materials call for a better understanding of the weak “physisorption” interactions of the hydrogen molecule with other substances.

Charge transfer to and from the H₂ molecule has an important role throughout the chemistry of physisorbed H₂. More specifically, there are two important CT mechanisms: (1) H₂ is a weak Lewis base where charge is accepted from the adsorbent to the $\sigma^*(\text{H}_2)$ orbital (Figure 11a,c). For cases in

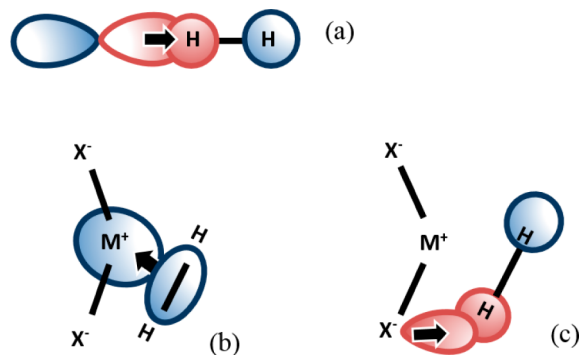


Figure 11. Charge transfer in weakly interacting H₂ physisorption complexes.

which this mechanism is important, the H₂ is oriented “head-on” toward the charge donor, increasing the acceptor’s overlap with the $\sigma^*(\text{H}_2)$ orbital and the H–H stretch becomes IR-allowed. This dative interaction can be as weak as -0.5 kJ/mol, but can also be much stronger. (2) H₂ is a weak Lewis acid that donates charge from its σ orbital (Figure 11b). Where this mechanism is important, the H₂ is positioned “side-on” toward the charge acceptor, increasing the acceptor’s overlap with the $\sigma(\text{H}_2)$ orbital.

Polarization can also have a significant contribution to the physisorption of H₂, inducing electrostatic moments on H₂, and enabling an attractive electrostatic interaction with the linker. A good H₂ polarizing environment should have a strong local dipole (Figure 12a) or quadrupole (Figure 12b,c) moment. Higher moments of the polarizing environment are not able to induce a significant change in the electrostatic distribution (Figure 12d).

In considering the interactions of H₂ with MOF linkers, we have evaluated three physisorption motifs: (A) Nonmetalated linkers. (B) Fully coordinated metalated linkers. (C) Metalated linkers with strong electrostatic moments.

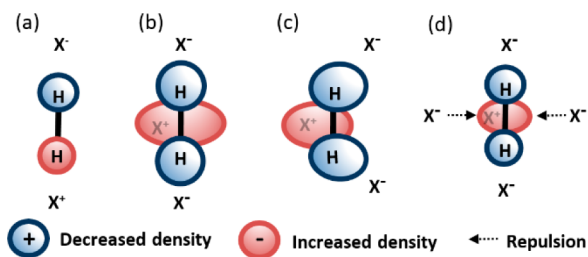


Figure 12. Polarization of hydrogen molecule by the electrostatic environment. The H₂ molecule is placed above a positive charged ion, accept for case (a).

For case (A), where no metals exist and there are no acceptor or donor groups on the linker, weak CT and dispersion are the only attractive forces. The typical binding energy is about -3 to -5 kJ/mol. For case (B), where closed shell coordinated metal ions are present, H₂ donates charge into diffuse Rydberg-like orbitals on the metal in addition to the forces mentioned in (A). The degree of CT is dependent on the accessibility of the metal ion to the H₂ molecule, such that planar metalated linker complexes have stronger M–H₂ interactions than tetrahedral complexes. Polarization is small, due to the screening of the metal ion by proximal counterions or, in the case of planar complexes, existence of an octupole moment that is incompatible with H₂. For case (C), due the existence of strong electrostatic moments that are compatible with H₂, the attraction mechanism is mostly electrostatic, where the H₂ is polarized and attracted by electrostatic forces to the linker. This important attraction mechanism is “physical” and the H₂ is neither an acid nor a base with respect to the linker. The polarization mechanism is supplemented by significant $\sigma(\text{H}_2) \rightarrow$ metal CT, which is relatively strong due to the low coordination environment, allowing for a shorter distance between the H₂ and the metal and good overlap between the orbitals.

An important conclusion of this work concerns the design of metal-decorated MOFs: Assuming that no strong orbital interactions occur between the H₂ and the metal center, such that physisorption is the main interaction, only motif (C) has the potential to achieve sufficiently strong interaction energies to reach the desired target range. The preparation of metal sites with the proper structure, leaving the metal mostly exposed is expected to be a major experimental challenge, as these metal sites are expected to have interactions with solvent molecules that are an order of magnitude or more stronger than the interaction with H₂. These solvent molecules, if they cannot be displaced, would disrupt metal–H₂ interactions by impeding the electric fields and blocking CT favorable binding sites. A possible approach for circumventing the solvent problem is to use a solvent-free gas phase metalation, which appears feasible for aluminum.

ASSOCIATED CONTENT

Supporting Information

Additional computational details and optimized geometries. This material is available free of charge via the Internet at <http://pubs.acs.org>.

AUTHOR INFORMATION

Corresponding Author

mhg@cchem.berkeley.edu

Notes

The authors declare no competing financial interest.

ACKNOWLEDGMENTS

We would like to thank Dr. Shane Yost, Narbe Mardirossian and Jarad Mason for their helpful comments and discussion. This research was funded by the United States Department of Energy, Energy Efficiency and Renewable Energy, Hydrogen and Fuel Cell Program.

REFERENCES

- Li, B.; Wen, H.-M.; Zhou, W.; Chen, B. *J. Phys. Chem. Lett.* **2014**, *5*, 3468.

- (2) Zhou, H.-C.; Long, J. R.; Yaghi, O. M. *Chem. Rev.* **2012**, *112*, 673.
- (3) Yoon, M.; Srirambalaji, R.; Kim, K. *Chem. Rev.* **2012**, *112*, 1196.
- (4) Li, J.-R.; Sculley, J.; Zhou, H.-C. *Chem. Rev.* **2012**, *112*, 869.
- (5) Suh, M. P.; Park, H. J.; Prasad, T. K.; Lim, D.-W. *Chem. Rev.* **2012**, *112*, 782.
- (6) Das, M. C.; Xiang, S.; Zhang, Z.; Chen, B. *Angew. Chem., Int. Ed.* **2011**, *50*, 10510.
- (7) Cohen, S. M. *Chem. Rev.* **2012**, *112*, 970.
- (8) Bloch, E. D.; Britt, D.; Lee, C.; Doonan, C. J.; Uribe-Romo, F. J.; Furukawa, H.; Long, J. R.; Yaghi, O. M. *J. Am. Chem. Soc.* **2010**, *132*, 14382.
- (9) Evans, J. D.; Sumby, C. J.; Doonan, C. J. *Chem. Soc. Rev.* **2014**, *43*, 5933.
- (10) Chen, B.; Zhao, X.; Putkham, A.; Hong, K.; Lobkovsky, E. B.; Hurtado, E. J.; Fletcher, A. J.; Thomas, K. M. *J. Am. Chem. Soc.* **2008**, *130*, 6411.
- (11) Dincă, M.; Long, J. R. *Angew. Chem., Int. Ed.* **2008**, *47*, 6766.
- (12) Sumida, K.; Stück, D.; Mino, L.; Chai, J.-D.; Bloch, E. D.; Zavorotynska, O.; Murray, L. J.; Dincă, M.; Chavan, S.; Bordiga, S.; Head-Gordon, M.; Long, J. R. *J. Am. Chem. Soc.* **2013**, *135*, 1083.
- (13) Kubas, G. J. *Chem. Rev.* **2007**, *107*, 4152.
- (14) Saillard, J. Y.; Hoffmann, R. *J. Am. Chem. Soc.* **1984**, *106*, 2006.
- (15) Kubas, G. J. *J. Organomet. Chem.* **2001**, *635*, 37.
- (16) Lochan, R. C.; Head-Gordon, M. *Phys. Chem. Chem. Phys.* **2006**, *8*, 1357.
- (17) Lochan, R. C.; Khaliullin, R. Z.; Head-Gordon, M. *Inorg. Chem.* **2008**, *47*, 4032.
- (18) Murray, L. J.; Dincă, M.; Long, J. R. *Chem. Soc. Rev.* **2009**, *38*, 1294.
- (19) Civalieri, B.; Napoli, F.; Noël, Y.; Roetti, C.; Dovesi, R. *CrystEngComm* **2006**, *8*, 364.
- (20) Lee, T. B.; Kim, D.; Jung, D. H.; Choi, S. B.; Yoon, J. H.; Kim, J.; Choi, K.; Choi, S.-H. *Catal. Today* **2007**, *120*, 330.
- (21) Sillar, K.; Hofmann, A.; Sauer, J. *J. Am. Chem. Soc.* **2009**, *131*, 4143.
- (22) Planas, N.; Dzubak, A. L.; Poloni, R.; Lin, L.-C.; McManus, A.; McDonald, T. M.; Neaton, J. B.; Long, J. R.; Smit, B.; Gagliardi, L. *J. Am. Chem. Soc.* **2013**, *135*, 7402.
- (23) Verma, P.; Xu, X.; Truhlar, D. G. *J. Phys. Chem. C* **2013**, *117*, 12648.
- (24) Xiao, D. J.; Bloch, E. D.; Mason, J. A.; Queen, W. L.; Hudson, M. R.; Planas, N.; Borycz, J.; Dzubak, A. L.; Verma, P.; Lee, K.; Bonino, F.; Crocellà, V.; Yano, J.; Bordiga, S.; Truhlar, D. G.; Gagliardi, L.; Brown, C. M.; Long, J. R. *Nat. Chem.* **2014**, *6*, 590.
- (25) Bloch, E. D.; Hudson, M. R.; Mason, J. A.; Chavan, S.; Crocellà, V.; Howe, J. D.; Lee, K.; Dzubak, A. L.; Queen, W. L.; Zadrozny, J. M.; Geier, S. J.; Lin, L.-C.; Gagliardi, L.; Smit, B.; Neaton, J. B.; Bordiga, S.; Brown, C. M.; Long, J. R. *J. Am. Chem. Soc.* **2014**, *136*, 10752.
- (26) Li, H.; Eddaoudi, M.; O'Keeffe, M.; Yaghi, O. M. *Nature* **1999**, *402*, 276.
- (27) Forster, P. M.; Eckert, J.; Chang, J.-S.; Park, S.-E.; Férey, G.; Cheetham, A. K. *J. Am. Chem. Soc.* **2003**, *125*, 1309.
- (28) Forster, P. M.; Eckert, J.; Heiken, B. D.; Parise, J. B.; Yoon, J. W.; Jhung, S. H.; Chang, J.-S.; Cheetham, A. K. *J. Am. Chem. Soc.* **2006**, *128*, 16846.
- (29) FitzGerald, S. A.; Allen, K.; Landerman, P.; Hopkins, J.; Matters, J.; Myers, R.; Rowsell, J. L. C. *Phys. Rev. B: Condens. Matter Mater. Phys.* **2008**, *77*, 224301.
- (30) Vitillo, J. G.; Regli, L.; Chavan, S.; Ricciardi, G.; Spoto, G.; Dietzel, P. D. C.; Bordiga, S.; Zecchina, A. *J. Am. Chem. Soc.* **2008**, *130*, 8386.
- (31) Khaliullin, R. Z.; Cobar, E. A.; Lochan, R. C.; Bell, A. T.; Head-Gordon, M. *J. Phys. Chem. A* **2007**, *111*, 8753.
- (32) Horn, P. R.; Sundstrom, E. J.; Baker, T. A.; Head-Gordon, M. *J. Chem. Phys.* **2013**, *138*, 134119.
- (33) Shao, Y.; Fusti-Molnar, L.; Jung, Y.; Kussmann, J.; Ochsenfeld, C.; Brown, S. T.; Gilbert, A. T. B.; Slipchenko, L. V.; Levchenko, S. V.; O'Neill, D. P.; DiStasio, R. A., Jr.; Lochan, R. C.; Wang, T.; Beran, G. J. O.; Besley, N. A.; Herbert, J. M.; Yeh Lin, C.; Van Voorhis, T.; Hung Chien, S.; Sodt, A.; Steele, R. P.; Rassolov, V. A.; Maslen, P. E.; Korambath, P. P.; Adamson, R. D.; Austin, B.; Baker, J.; Byrd, E. F. C.; Dachsels, H.; Doerksen, R. J.; Dreuw, A.; Dunietz, B. D.; Dutoi, A. D.; Furlani, T. R.; Gwaltney, S. R.; Heyden, A.; Hirata, S.; Hsu, C.-P.; Kedziora, G.; Khalliulin, R. Z.; Klunzinger, P.; Lee, A. M.; Lee, M. S.; Liang, W.; Lotan, I.; Nair, N.; Peters, B.; Proynov, E. I.; Pieniazek, P. A.; Min Rhee, Y.; Ritchie, J.; Rosta, E.; David Sherrill, C.; Simmonett, A. C.; Subotnik, J. E.; Lee Woodcock, H., III; Zhang, W.; Bell, A. T.; Chakraborty, A. K.; Chipman, D. M.; Keil, F. J.; Warshel, A.; Hehre, W. J.; Schaefer, H. F., III; Kong, J.; Krylov, A. I.; Gill, P. M. W.; Head-Gordon, M. *Phys. Chem. Chem. Phys.* **2006**, *8*, 3172.
- (34) Gianinetti, E.; Raimondi, M.; Tornaghi, E. *Int. J. Quantum Chem.* **1996**, *60*, 157.
- (35) Khaliullin, R. Z.; Head-Gordon, M.; Bell, A. T. *J. Chem. Phys.* **2006**, *124*, 204105.
- (36) Khaliullin, R. Z.; Bell, A. T.; Head-Gordon, M. *J. Chem. Phys.* **2008**, *128*, 184112.
- (37) Grimme, S. *J. Comput. Chem.* **2006**, *27*, 1787.
- (38) Grimme, S.; Antony, J.; Ehrlich, S.; Krieg, H. *J. Chem. Phys.* **2010**, *132*, 154104.
- (39) Weigend, F.; Ahlrichs, R. *Phys. Chem. Chem. Phys.* **2005**, *7*, 3297.
- (40) Rappoport, D.; Furche, F. *J. Chem. Phys.* **2010**, *133*, 134105.
- (41) Mardirossian, N.; Head-Gordon, M. *Phys. Chem. Chem. Phys.* **2014**, *16*, 9904.
- (42) Rezáč, J.; Hobza, P. *J. Chem. Theory Comput.* **2013**, *9*, 2151.
- (43) Vydrov, O. A.; Voorhis, T. V. *J. Chem. Phys.* **2010**, *133*, 244103.
- (44) Ma, L.; Falkowski, J. M.; Abney, C.; Lin, W. *Nat. Chem.* **2010**, *2*, 838.
- (45) Carson, F.; Agrawal, S.; Gustafsson, M.; Bartoszewicz, A.; Moraga, F.; Zou, X.; Martín-Matute, B. *Chem.—Eur. J.* **2012**, *18*, 15337.
- (46) Fei, H.; Cohen, S. M. *Chem. Commun.* **2014**, *50*, 4810.
- (47) Bohnsack, A. M.; Ibarra, I. A.; Bakhmutov, V. I.; Lynch, V. M.; Humphrey, S. M. *J. Am. Chem. Soc.* **2013**, *135*, 16038.
- (48) Wang, L.; Sun, Y.; Sun, H. *Faraday Discuss.* **2011**, *151*, 143.
- (49) Getman, R. B.; Miller, J. H.; Wang, K.; Snurr, R. Q. *J. Phys. Chem. C* **2011**, *115*, 2066.
- (50) Brand, S. K.; Colón, Y. J.; Getman, R. B.; Snurr, R. Q. *Microporous Mesoporous Mater.* **2013**, *171*, 103.
- (51) Tanabe, K. K.; Allen, C. A.; Cohen, S. M. *Angew. Chem., Int. Ed.* **2010**, *49*, 9730.
- (52) Fei, H.; Shin, J.; Meng, Y. S.; Adelhardt, M.; Sutter, J.; Meyer, K.; Cohen, S. M. *J. Am. Chem. Soc.* **2014**, *136*, 4965.
- (53) Wheeler, S. E. *J. Am. Chem. Soc.* **2011**, *133*, 10262.
- (54) Wheeler, S. E. *Acc. Chem. Res.* **2013**, *46*, 1029.
- (55) Mondloch, J. E.; Bury, W.; Fairen-Jimenez, D.; Kwon, S.; DeMarco, E. J.; Weston, M. H.; Sarjeant, A. A.; Nguyen, S. T.; Stair, P. C.; Snurr, R. Q.; Farha, O. K.; Hupp, J. T. *J. Am. Chem. Soc.* **2013**, *135*, 10294.